Radiology

Micro-PET Imaging of β-Glucuronidase Activity by the Hydrophobic Conversion of a Glucuronide Probe[1]

Shey-Cherng Tzou, PhD
Steve Roffler, PhD
Kuo-Hsiang Chuang, MS
Hsin-Pei Yeh, MS
Chien-Han Kao, MS
Yu-Cheng Su, MS
Chiu-Min Cheng, PhD
Wei-Lung Tseng, PhD
Jentaie Shiea, PhD
I-Hong Harm, MS
Kai-Wen Cheng, BS
Bing-Mae Chen, MS
Jeng-Jong Hwang, PhD
Tian-Lu Cheng, PhD
Hsin-Ell Wang, PhD

Purpose: To develop a new glucuronide probe for micro–positron emission topography (PET) that can depict β-glucuronidase (βG)-expressing tumors in vivo.

Materials and Methods: All animal experiments were preapproved by the Institutional Animal Care and Use Committee. A βG-specific probe was generated by labeling phenolphthalein glucuronide (PTH-G) with iodine 131 (^{131}I) or ^{124}I. To test the specificity of the probe in vitro, ^{124}I-PTH-G was added to CT26 and βG-expressing CT26 (CT26/βG) cells. Mice bearing CT26 and CT26/βG tumors ($n = 6$) were injected with ^{124}I-PTH-G and subjected to micro-PET imaging. A βG-specific inhibitor D-saccharic acid 1,4-lactone monohydrate was used in vitro and in vivo to ascertain the specificity of the glucuronide probes. Finally, the biodistributions of the probes were determined in selected organs after injection of ^{131}I-PTH-G to mice bearing CT26 and CT26/βG tumors ($n = 14$). Differences in the radioactivity in CT26 and CT26/βG tumors were analyzed with the Wilcoxon signed rank test.

Results: ^{124}I-PTH-G was selectively converted to ^{124}I-PTH (phenolphthalein), which accumulated in CT26/βG cells and tumors in vitro. The micro-PET images demonstrated enhanced activity in CT26/βG tumors resulting from βG-mediated conversion and trapping of the radioactive probes. Accumulation of radioactive signals was 3.6-, 3.4-, and 3.3-fold higher in the CT26/βG tumors than in parental CT26 tumors at 1, 3, and 20 hours, respectively, after injection of the probe (for all the three time points, $P < .05$).

Conclusion: Hydrophilic-hydrophobic conversion of ^{124}I-PTH-G probe can aid in imaging of βG-expressing tumors in vivo.

[1] From the Faculty of Biomedical Science and Environmental Biology (S.C.T., C.M.C., I.H.H., K.W.C., T.L.C.) and Graduate Institute of Medicine (K.H.C., C.H.K.), Kaohsiung Medical University, 100 Shih-Chuan 1st Road, Kaohsiung 807, Taiwan; Institute of Biomedical Sciences, Academia Sinica, Taipei, Taiwan (S.R., B.M.C.); Faculty of Biomedical Imaging and Radiological Sciences (H.P.Y., J.J.H., H.E.W.) and Institute of Microbiology and Immunology (Y.C.S.), National Yang-Ming University, Taipei, Taiwan; Department of Chemistry, National Sun Yat-Sen University, Kaohsiung, Taiwan (W.L.T., J.S.); and National Sun Yat-sen University-Kaohsiung Medical University Joint Research Center, Kaohsiung, Taiwan (W.L.T., J.S., T.L.C.).
Received December 1, 2008; revision requested January 21 2009; revision received February 17; accepted March 13; final version accepted March 24. Supported by the National Research Program for Genomic Medicine, the National Science Council, Taipei, Taiwan (grants NSC 96-3112-B-037-001 and NSC 95-2311-B001-068-MY3), Academia Sinica (grant AS-98-TP-B09) and the National Health Research Institutes (grant NHRI-EX97-9624SI).
Address correspondence to T.L.C. (e-mail: *tlcheng@kmu.edu.tw*).

Enzymes that are selectively expressed at or targeted to tumor sites can be used to convert relatively nontoxic prodrugs into active, cytotoxic drugs to enhance antitumor activity and reduce systemic toxicity, compared with conventional chemotherapy. β-Glucuronidase (βG) is an attractive enzyme for activation of antineoplastic prodrugs. Glucuronide prodrugs of several anticancer drugs have been synthesized, including doxorubicin (1,2), etoposide (3), camptothecin analogs (4,5), paclitaxel (6), docetaxel (7) and alkylating agents (8,9). In fact, glucuronide derivatives of almost any antineoplastic agent can be synthesized by using linkers between a drug and a glucuronide group (5,7). Glucuronide prodrugs are relatively nontoxic due to the hydrophilic nature of the glucuronide group, which prevents them from entering cells and, thus, from contacting lysosomal βG (10). In addition, glucuronide prodrugs have been shown to produce potent antitumor activity in antibody-directed enzyme prodrug therapy (8,11), gene-directed enzyme prodrug therapy (12–14), bacterially directed prodrug therapy (15), as well as directly in prodrug monotherapy (4,16), which relies on the presence of elevated levels of βG in the tumor interstitial space (16,17).

Endogenous βG activity in tumors varies widely (18,19). In addition, accumulation of targeted or expressed βG in tumors may change over time. The ability to image intratumoral βG activity in tumors will greatly aid in the design of personalized glucuronide prodrug treatment and greatly improve βG-based targeted therapy. However, current βG probes are only suitable for in vitro studies but not yet available for in vivo imaging of βG activity (20–24). To be clinically useful, development of glucuronide probes for more sensitive imaging technologies such as positron emission tomography (PET) will aid in the imaging of βG activity in vivo for glucuronide prodrug therapy.

Our purpose in this study was to develop a new glucuronide probe for micro-PET imaging that can depict βG-expressing tumors in vivo.

Advances in Knowledge

- The hydrophilic-hydrophobic conversion of a proactive glucuronide probe by β-glucuronidase (βG) can be used to detect βG activity in vivo.
- This hydrophilic-hydrophobic conversion may be adopted to design probes for other enzyme system(s) that show preferential up-regulation in the tumor site, for instance, metallomatrix proteases.

Implication for Patient Care

- The development of new glucuronide probes for PET may aid in the diagnosis of βG-expressing cancers, identifying those cancer patients who are suitable for glucuronide prodrug therapy in the future.

Materials and Methods

Cells and Animals

CT26 murine colon carcinoma and βG-expressing CT26 (CT26/βG) cells (24) were cultured in Dulbecco's Minimal Essential Medium (DMEM) (Sigma-Aldrich, St Louis, Mo) supplemented with 10% heat-inactivated bovine calf serum, 100 U/mL penicillin, and 100 μg/mL streptomycin at 37°C in a 5% CO_2 atmosphere. Female BALB/c mice, 6–8 weeks old, were purchased from the National Laboratory Animal Center (Taipei, Taiwan). To avoid excessive uptake of the radioiodinated agents by the thyroid glands, all mice were pretreated with 0.2% Lugol solution (Sigma-Aldrich) in their drinking water for 2 days prior to the injection of the radioiodinated probes, as previously described (25). The animal experiments were conducted in accordance with the standards set forth by the National Yang-Ming University Institutional Animal Care and Use Committee.

Generation of ^{131}I- or ^{124}I-PTH-G Probes

To initiate labeling, 8 μL of chloramine-T solution (5 mg/mL in deionized H_2O) were added to a mixture of 50 μg of phenolphthalein glucuronide (PTH-G) (Sigma-Aldrich), iodine 124 (^{124}I) NaI (3.7–37 MBq; IBA Molecular, Louvain-La-Neuve, Belgium), or ^{131}I NaI solution (Nuclear Science and Technology Development Center, National Tsing Hua University, Taiwan) in 50 μL of 0.5 mol/L ammonium acetate buffer (pH 3.4) and vortexed intermittently at room temperature for 2 minutes. Ten microliters of 1 mol/L $Na_2S_2O_3$ were added to stop the reaction. The reaction mixture was loaded into a preconditioned Sep-Pak PLus C18 cartridge (Waters, Milford, Mass) and washed with 5 mL water to remove free radioactive iodide. ^{131}I-PTH-G or ^{124}I-PTH-G was eluted with 3 mL of ethanol and water (2:1 vol/vol) and evaporated to dryness under a gentle stream of nitrogen at 100°C. The specific activity of ^{124}I-PTH-G and ^{131}I-PTH-G was about 555 MBq/μmol. The radiochemical purity was greater than 95%, as determined (H.P.Y., W.L.T., J.S., and H.E.W., with 3, 10, 24, and 20 years of experience in chemical labeling and analysis) at radio–thin-layer chromatography

Published online
10.1148/radiol.2523082055

Radiology 2009; 252:754–762

Abbreviations:
βG = β-glucuronidase
DMEM = Dulbecco's Minimal Essential Medium
DOTA = tetraazacyclododecane tetraacetic acid
PTH = phenolphthalein
PTH-G = phenolphthalein glucuronide

Author contributions:
Guarantors of integrity of entire study, S.C.T., S.R., K.H.C., H.P.Y., Y.C.S., W.L.T., I.H.H., K.W.C., J.J.H., T.L.C., H.E.W.; study concepts/study design or data acquisition or data analysis/interpretation, all authors; manuscript drafting or manuscript revision for important intellectual content, all authors; approval of final version of submitted manuscript, all authors; literature research, S.C.T., S.R., K.H.C., H.P.Y., C.H.K., C.M.C., W.L.T., I.H.H., K.W.C., T.L.C., H.E.W.; experimental studies, all authors; statistical analysis, S.C.T., K.H.C., H.P.Y., C.H.K., Y.C.S., C.M.C., I.H.H., K.W.C., T.L.C., H.E.W.; and manuscript editing, S.C.T., S.R., K.H.C., H.P.Y., C.H.K., C.M.C., J.S., I.H.H., K.W.C., T.L.C., H.E.W.

Authors stated no financial relationship to disclose.

by using an aluminum sheet coated with silica powder, separated with an aqueous ethanol and water (1:1 vol/vol) mobile phase, then scanned with an AR 2000 scanner (Bioscan, Washington, DC).

Hydrophobic Conversion of PTH-G into PTH by βG-expressing Cells and Tumors

CT26 or CT26/βG cells were stained for βG activity with the β-Glucuronidase Reporter Gene Staining Kit (Sigma-Aldrich) or with 10 μmol/L PTH-G in 0.5-mL serum-free DMEM (pH 6.5) for 3 hours. The reddish-brown phenolphthalein (PTH) precipitate was visualized with the addition of 2 μL triethylamine. The cells were then examined under an upright microscope (BX41; Olympus, Melville, NY). To assess specific hydrolysis of PTH-G by βG ex vivo, CT26 or CT26/βG tumors were excised and embedded in a compound (Tissue-Tek OCT; Sakara Finetek, Torrance, Calif) in liquid nitrogen and sectioned into 10-μm slices. Adjacent tumor sections were stained (C.H.K., B.M.C., and C.M.C., with 4, 20, and 10 years of experience in cell culture) for βG activity with X-GlcA (Sigma-Aldrich) and PTH-G.

Metabolism of ^{131}I-PTH-G in Vitro

CT26/βG or parental CT26 cells (1×10^6 cells per well) cultured in six-well plates were washed three times with phosphate-buffered saline and then incubated with ^{131}I-PTH-G (370 kBq of solution per well) in 0.5-mL serum-free DMEM at 37°C. Samples were periodically removed at 15, 30, 60, 120, and 240 minutes, were blotted onto an aluminum sheet precoated with silica, and were dried. ^{131}I-PTH-G and ^{131}I-PTH were then separated on the silica by a mobile phase composed of ethanol and water (1:1 vol/vol). The radioactivity of ^{131}I-PTH-G and ^{131}I-PTH was measured (C.H.K., B.M.C., and C.M.C.) with a radio–thin-layer chromatography plate scanner.

Specific Conversion and Accumulation of ^{124}I-PTH-G by βG

To assess specific hydrolysis of radioactive probes by βG in vitro, graded amounts of ^{124}I-PTH-G in 50-μL per-well serum-free DMEM (pH 6.5) were added to 96-well microtiter plates containing live CT26 or CT26/βG cells for 1 hour. To establish the specificity of ^{124}I-PTH-G, D-saccharic acid 1,4-lactone monohydrate (SAL, a specific βG inhibitor; Sigma-Aldrich [26]) was added to the cells to a final concentration of 0.5 mg/mL 45 minutes before the addition of ^{124}I-PTH-G. The wells were washed to remove free probe before the cells were collected by means of treatment with trypsin. The radioactivity of the cells was then measured (C.H.K., B.M.C., and C.M.C.) in a gamma counter (1470 Wizard, Wallac, Turku, Finland).

Serum Half-Live of ^{131}I-PTH-G

BALB/c mice (n = 5) were intravenously injected with 1.85-MBq ^{131}I-PTH-G, and blood samples were removed from the tail vein at 5, 10, 15, 30, 60, 120, 240, 480, and 1440 minutes. The blood was weighed on an analytical balance and assayed for radioactivity in a gamma counter. Results are expressed as the percentage of injected dose per gram of tissue. The initial and terminal half-lives of the probe were estimated (Y.C.S. and K.H.C., both with 5 years of experience in half-life determination) by fitting the data to a two-phase exponential decay model with use of software (Prism 4; Graphpad Software, San Diego, Calif).

In Vivo Micro-PET Imaging

BALB/c mice (n = 3) bearing established CT26 and βG-expressing CT26 tumors (200–300 mm^3) in their left and right chest regions, respectively, were anesthetized with halothane vapor by using a vaporizer system and then were intravenously injected with 3700 kBq (in 100 μL) ^{124}I-PTH-G. To test the specificity of ^{124}I-PTH-G in vivo, D-saccharic acid 1,4-lactone monohydrate (1 g per kilogram of body weight) was intraperitoneally injected into the mice (n = 3) 1 hour before ^{124}I-PTH-G injection. PET imaging was sequentially performed at 1, 3, and 20 hours. The tumor-bearing mice were positioned in a micro-PET scanner (R4; Concorde Microsystems, Knoxville, Tenn) with their long axis parallel to the transaxial plane of the scanner. The scanner has a computer-controlled bed with a 10.8-cm transaxial and 8-cm axial field of view. It has no septa and operates exclusively in a three-dimensional list mode. All raw data were first sorted into three-dimensional sinograms, followed by Fourier rebinning and ordered-subsets expectation maximization image reconstruction. Fully three-dimensional list-mode data were collected by using an energy window of 350–750 keV and a time window of 6 nsec. Image pixel size was 0.85 mm transaxially, with a 1.21-mm section thickness (SCT., K.H.C., I.H.H., and H.E.W., with 2, 4, 2, and 20 years of experience in imaging studies).

Whole-Body Autoradiography in Mice

For autoradiography, the tumor-bearing mice (n = 3) were intravenously injected with 3700 kBq (100 μL) of ^{131}I-PTH-G. Animals were sacrificed by means of chloroform inhalation 3 hours after injection and were immediately dipped into isopentane (Nacalai Tesque, Kyoto, Japan), which was prechilled at liquid nitrogen temperature. The whole carcass was frozen for 1–2 minutes, depending on body size. The frozen carcass was then embedded on a cryostat holder with 4% carboxylmethylcellulose (27). Coronal sectioning was performed with a slice thickness of 30 μm. Slices attached on the microscopic slides were air dried at room temperature, applied to the imaging plates (BAS cassette 2040; Fujifilm, Tokyo, Japan), and exposed for about 36 hours. After exposure, the imaging plates were assayed with a FLA5000 reader (Fujifilm) to acquire the phosphor images. The intensity of the linear arbitrary unit of the CT-26 tumor and the CT26/βG tumor was measured (K.H.C., Y.C.S., I.H.H., and H.E.W., with 4, 4, 2, and 20 years of experience in autoradiography in mice) with Image Gauge (Version 5.0, Science Lab 2001; Fujifilm).

Detection of βG Activity in Necrotizing Tumor

BALB/c mice (n = 3) bearing CT26 and CT26/βG tumors (~400 mm^3) were intravenously injected with 3700 kBq of ^{131}I-PTH-G and sacrificed 3 hours later. Tumors were dissected, embedded in a compound (Tissue-Tek OCT), and snap frozen in liquid nitrogen. Consecutive sections were obtained for autoradiog-

raphy, βG enzyme assay (both 20 μm), and histologic examination with hematoxylin-eosin (10 μm) (SCT., I.H.H., K.W.C., and J.J.H., with 8, 2, 2, and 20 years of experience in histology). The results of autoradiography and βG enzyme activity were then matched to the necrotic regions at histologic examination.

Biodistribution of ^{131}I-PTH-G and ^{131}I-PTH

Tumor-bearing female BALB/c mice were intravenously injected with 2220-kBq (in 100 μL) ^{131}I-PTH-G or ^{131}I-PTH. Animals were sacrificed after anesthesia with pentobarbital (65 mg/kg) at 1 (n = 3), 3 (n = 5), and 20 (n = 6) hours. Radioactivity in the tumors and other internal organs was measured with a multichannel gamma counter (K.H.C., Y.C.S., I.H.H., and H.E.W., with 5, 5, 2, and 21 years experience in biodistribution study in mice). The accumulation of radioactivity in tissues was normalized to sample weight and expressed as percentage of injected dose per gram of tissue.

Statistical Analysis

The radioactivity of the CT26/βG tumors and parental CT26 tumors was recorded in the biodistribution analysis. Differences in radioactivity between CT26/βG and CT26 tumors located on the same mouse were analyzed (SCT., S.R., and T.L.C., with 4, 28, and 18 years experience of data analysis) by using the Wilcoxon signed rank test. P values of less than .05 were considered to indicate a statistically significant difference.

Results

Specific Conversion of PTH-G into PTH by βG-expressing Cells in Vitro and ex Vivo

In βG-expressing CT26 cells, βG is tethered to the surface of CT26 cells to allow free access of hydrophilic PTH-G molecules to the enzyme (Fig 1) (24). A reddish-brown PTH precipitate was apparent on the CT26/βG cells and tumors but not on parental CT26 cells and/or tumors after addition of PTH-G (Fig 2).

Specificity and Half-Life of the Iodinated PTH-G Probes

The percentage of ^{131}I-PTH-G steadily decreased over time, while the percentage of ^{131}I-PTH increased, which indicates specific conversion of ^{131}I-PTH-G to ^{131}I-PTH by βG (Fig 3). On the contrary, parental CT26 cells barely hydrolyzed ^{131}I-PTH-G to ^{131}I-PTH.

Cell-associated radioactivity steadily increased in CT26/βG cells but not in parental CT26 cells (Fig 3b). D-saccharic acid 1,4-lactone monohydrate hampered the accumulation of cell-associated radioactivity in CT26/βG cells, indicating that the conversion of ^{124}I-PTH-G to ^{124}I-PTH was blocked by inhibition of βG activity.

^{131}I-PTH-G concentration in serum followed a two-phase exponential decay kinetics, with an initial half-life of 11.1 minutes ± 4.3 (standard error) and a terminal half-life of 580 minutes ± 100 (Fig 3c).

Micro-PET Imaging of βG-expressing Tumors in Vivo

^{124}I-PTH-G selectively accumulated in CT26/βG tumors as early as 1 hour after injection (Fig 4a), suggesting that ^{124}I-PTH-G was preferentially converted into ^{124}I-PTH by the CT26/βG tumors. CT26 tumors, on the other hand, produced weak but distinct signals on micro-PET images. The region of interest ratio of CT26/βG to parental CT26 tumors was 3.9, 3.5, and 3 at 1, 3, and 20 hours, respectively. We also found strong signals in the abdomen of the mice (Fig 4). Although radioactivity selectively accumulated in CT26/βG tumors in mice pretreated with phosphate-buffered saline, D-saccharic acid 1,4-lactone monohydrate completely blocked the generation and accumulation of radioactivity in CT26/βG tumors (Fig 4b).

Biodistribution of ^{131}I-PTH-G in Vivo

Substantial radioactivity accumulated in CT26/βG tumors (Fig 5). We also found weaker but distinctive signals in CT26 tumors. Autoradiography and βG enzymatic activity matched in the necrotic areas in CT26 tumors as determined at histologic examination (Fig 5, bottom panel). We also found strong signals in the internal organs, notably in the gallbladder, liver, and intestines (Fig 5, top panel).

Mean radioactivity was significantly higher in CT26/βG tumors than in the parental CT26 tumors at 3 and 20 hours after injection of ^{131}I-PTH-G (P = .11 at 1 hour, P = .04 at 3 hours, P = .03 at 20 hours, Fig 6). On average, CT26/βG tumors accumulated 3.6-, 3.4-, and 3.3-fold more radioactivity than did parental CT26 tumors at 1, 3, and 20 hours, respectively. In contrast, injection of ^{131}I-PTH did not result in differential accumulation of radioactivity (P = .827

Figure 1

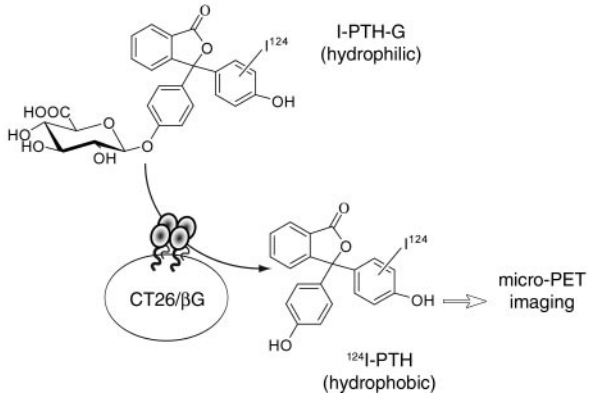

Figure 1: Schematic of the βG-based micro-PET imaging approach. βG tethered on the surface of CT26 (CT26/βG) cells can hydrolyze the glucuronide group from hydrophilic ^{124}I-PTH-G and convert it to hydrophobic ^{124}I-PTH, which can then accumulate in the cancer cells. The radiation from ^{124}I-PTH is then detected at micro-PET to diagnose βG activity in vivo for personalized glucuronide prodrug targeted therapy.

Figure 2

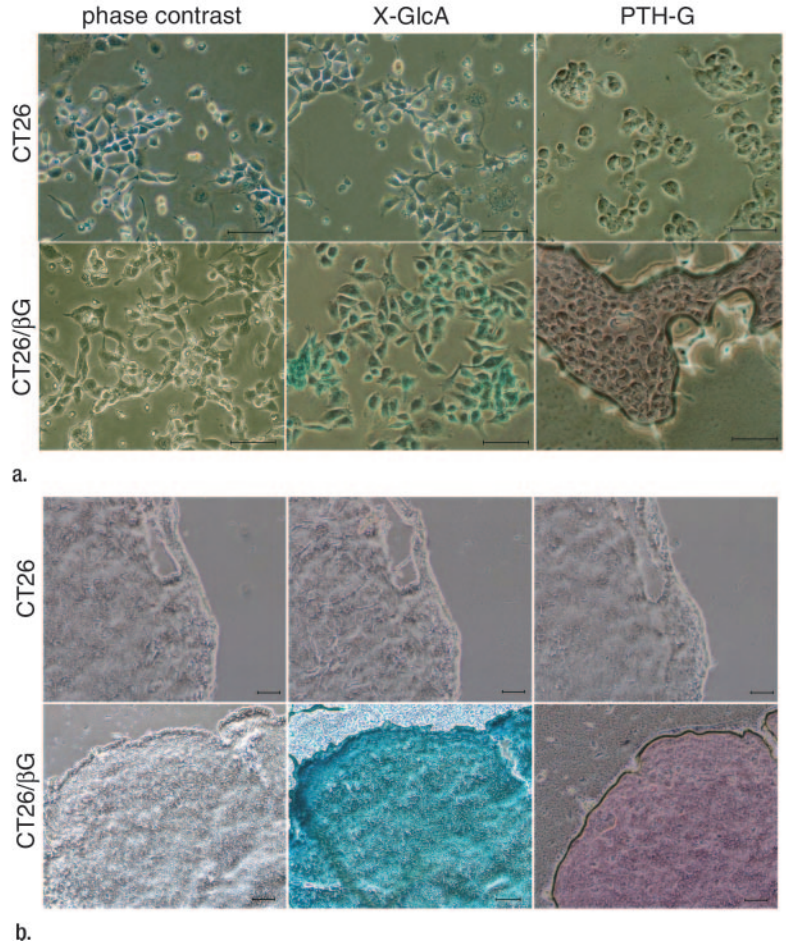

Figure 2: Specific conversion of hydrophilic PTH-G into hydrophobic PTH by βG in vitro and ex vivo. **(a)** PTH-G was incubated with CT26/βG cells or parental CT26 cells. The hydrolysis of PTH-G to PTH by βG is evident as reddish coat on the cell surface. **(b)** Sections of CT26 or CT26/βG tumors were incubated with PTH-G. The hydrolysis of PTH-G into PTH by βG is visualized as reddish coat. X-GlcA was added as a positive control for functional βG activity (blue color) in both assays. Scale bar = 10 μm (Original magnification, × 200).

Figure 3

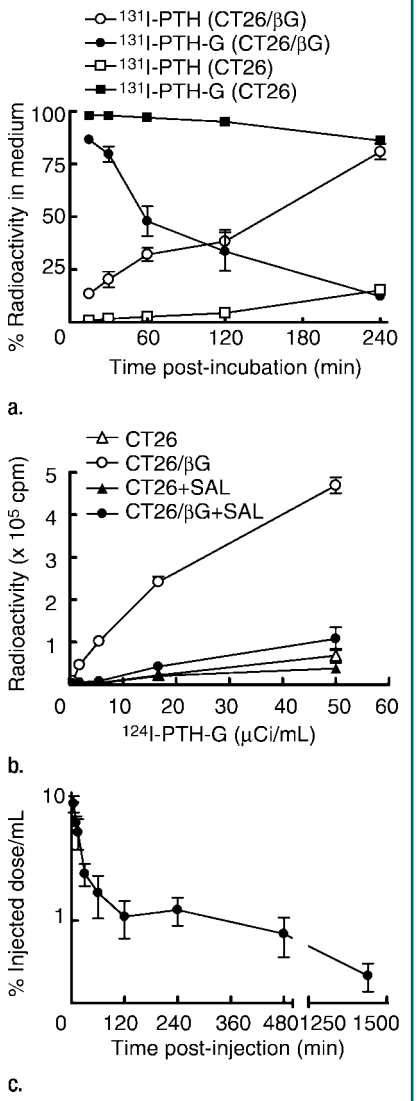

Figure 3: **(a)** Graph shows that the percentage of ^{131}I-PTH-G steadily decreased, while that of ^{131}I-PTH increased only in CT26/βG cells. **(b)** Graph shows that the radioactivity steadily increased in CT26/βG cells but not in parental CT26 cells. *SAL* = D-saccharic acid 1,4-lactone monohydrate. **(c)** Graph shows that ^{131}I-PTH-G concentration in serum followed two-phase exponential decay kinetics, with initial half-life of 11.1 minutes ± 4.3 and terminal half-life of 580 minutes ± 100. Error bar = standard error of triplicate determinations.

at 1 hour, $P = .827$ at 3 hours, $P = .275$ at 20 hours) (Fig 6b). As in the micro-PET studies, we found strong signals in the gallbladder, liver, and intestines.

Discussion

We have developed a strategy for the micro-PET imaging of βG activity based on the hydrophobic conversion of ^{124}I-PTH-G to ^{124}I-PTH. Our results show that CT26/βG cells and tumors selectively hydrolyzed and accumulated PTH-G and ^{124}I-PTH-G. The micro-PET images demonstrated enhanced activity in CT26/βG tumors. By using the βG-specific inhibitor D-saccharic acid 1,4-lactone monohydrate, we further validated that ^{124}I-PTH-G is a specific probe for βG activity in vitro and in vivo. The biodistribution of ^{131}I-PTH-G confirmed the preferential accumulation of ^{131}I-PTH in βG-expressing tumors. These results indicate that this method may potentially be a useful diagnostic tool for the detection of βG-expressing tumors to personalize glucuronide prodrug monotherapy or targeted therapy.

We noted radioactive signals in the CT26 tumors, gallbladder, and intestines. In the CT26 tumors, the radioactive signals were most likely generated by βG within the necrotic regions, which are known to contain high concentration of

βG (17,19). If ^{124}I- or ^{131}I-PTH-G was instead generated by other body sites and then traveled to CT26 tumors, one would expect a more homogeneous signal distribution within the tumors. This prediction, however, is not supported by our data. On the other hand, signals in gallbladder and intestines most likely resulted from excretion of glucuronide metabolites. Liver cells can uptake glucuronide conjugates such as ^{124}I-PTH-G from the blood by organic anion-transporting polypeptides expressed on the basolateral (sinusoidal) side of liver cells (28,29). For example, estradiol-17-β-D-glucuronide and telmisartan acylglucuronide are substrates for liver uptake by organic anion-transporting polypeptide family members (30–32). Once the glucuronide conjugates are within liver cells, Mrp2 (multiple resistance-associated protein 2) expressed on the apical (canicular) side of liver cells then pumps out glucuronide conjugates via the bile duct to the intestine (33). Anticancer drug metabolites, such as SN-38 glucuronide (a camptothecin derivative) and flavopiridol glucuronide, are secreted into the bile through the action of Mrp2 (34,35). βG in commensal flora present in the intestinal tract can hydrolyze glucuronide conjugates into their original forms. This is the mechanism underlying the severe diarrhea observed in cancer patients receiving CPT-11 (36).

Several methods can be considered to help overcome the nonspecific signal produced by bacterial βG and improve specific detection of βG-expressing tumors. First, before ^{124}I-PTH-G injection, mice can be pretreated with antibiotics to clear intestinal microbes, though it might lead to repopulation of pathogenic flora. Sec-

Figure 4

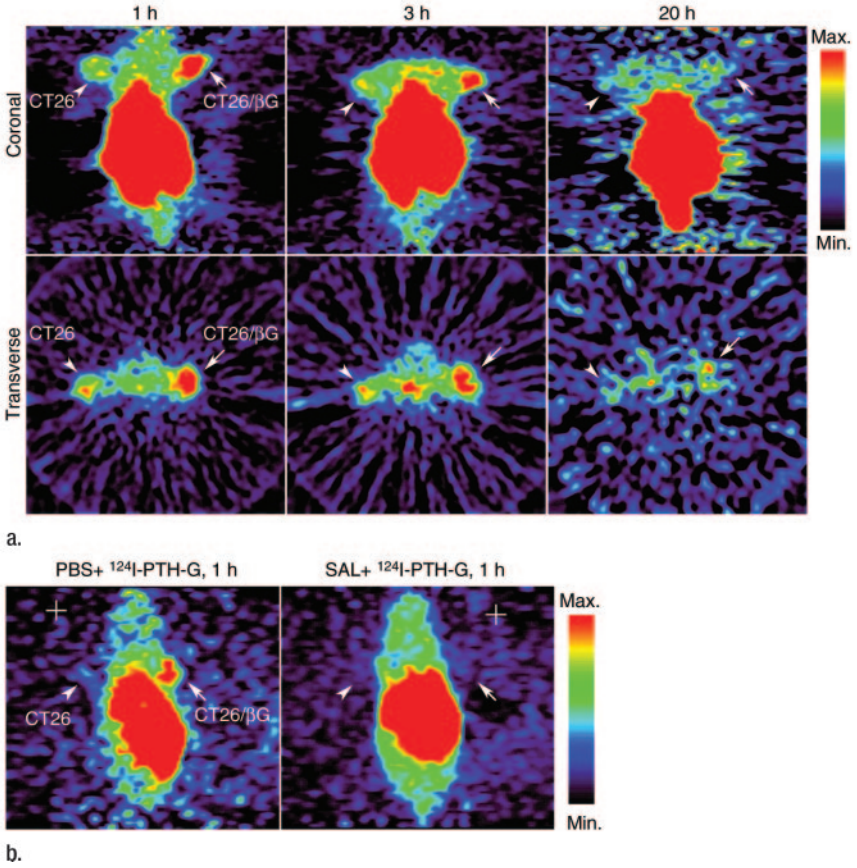

Figure 4: Micro-PET images of βG-expressing tumors in vivo. **(a)** Coronal and transverse images of BALB/c mice bearing CT26/βG (arrows) and parental CT26 (arrowheads) tumors 1, 3, and 20 hours after intravenous injection of ^{124}I-PTH-G. **(b)** Coronal images demonstrate the specificity of ^{124}I-PTH-G for βG activity. *PBS+ ^{124}I-PTH-G, 1 h* = Image obtained after injection of phosphate-buffered saline 1 hour prior to injection of ^{124}I-PTH-G, *SAL+ ^{124}I-PTH-G, 1 h* = image obtained after injection of D-saccharic acid 1,4-lactone monohydrate 1 hour prior to injection of ^{124}I-PTH-G.

Figure 5

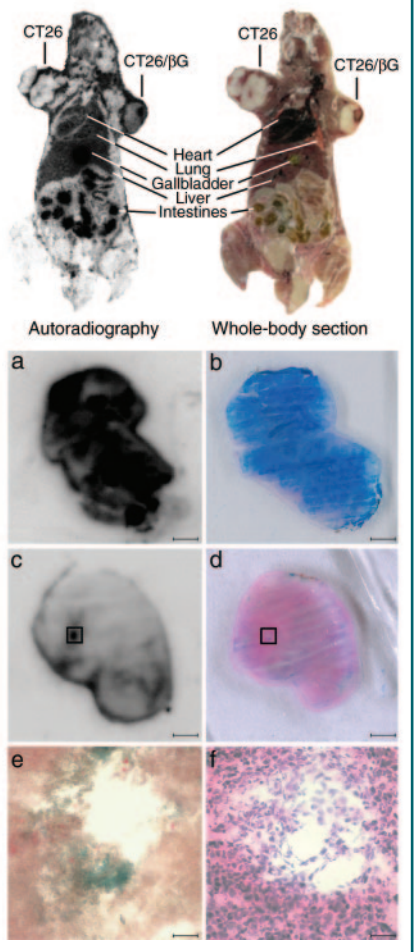

Figure 5: Top: Autoradiograph (left) and whole-body section (right) from a mouse bearing CT26/βG or parental CT26 tumors intravenously injected with ^{131}I-PTH-G. Bottom: Tumor-bearing mice injected with ^{131}I-PTH-G. *a, b,* CT26/βG and, *c–f,* CT26 tumors that were frozen sectioned for autoradiography *(a, c)*, βG activity *(b, d, e)*, and histologic analysis *(f)*. The boxed area in *d* is shown at higher magnification than in *e* and *f*. Disintegrated and amorphonuclear cells within the cavity suggest that it represents a necrotic region in the CT26 tumor *(f)*. Scale bar in *a* and *b* = 200 μm; *c–f* = 25 μm.

ond, PTH-G excretion may be shunted from the biliary to the urinary pathway. Repeated administration of acetaminophen can increase expression of Mrp3 and drive the elimination of xenobiotic glucuronides through the urinary pathway (37). Likewise, probenecid can inhibit Mrp2 and reduce biliary excretion of glucuronides (34,38). Increased urinary elimination may reduce the radioactivity retained in the intestines. Last, since PTH-G is likely excreted through the biliary pathway (39), PTH can be replaced with other compounds that exhibit predominately urinary excretion. In this regard, the relatively hydrophobic chelating agent tetraazacyclododecane tetraacetic acid (DOTA) is efficiently removed from the blood via the kidneys (40). Gallium 68–DOTA has been developed for cancer imaging with use of PET (41), which suggests that DOTA is an attractive candidate substitute for PTH.

Selective hydrolysis of a glucuronide probe to a hydrophobic reporter for PET imaging may be an effective strategy to detect βG activity in vivo. Conjugation of glucuronide groups usually increases the hydrophilicity of compounds (42,43). In addition, although βG is highly specific for the glucuronyl residue of glucuronide conjugates, it has little specificity for the conjugated aglycone (44), suggesting that a wide variety of glucuronide-imaging probes could be designed for PET, single photon emission computed tomography (SPECT), or magnetic resonance (MR) imaging. For example, a range of phenolic compounds, such resveratrols, could be glucuronidated and labeled with ^{124}I to form PET probes with unique properties. Similarly, glucuronide groups can be attached to hydrophobic derivatives of chelating agents such as DOTA for imaging (45). DOTA-glucuronide derivatives could chelate gadolinium or indium 111 to form imaging probes for the detection of βG activity by using MR imaging or SPECT, respectively. Thus, the concept of βG-specific conversion and accumulation of hydrophobic probes opens a new venue for the design of βG-detecting probes for imaging technologies commonly used in modern medicine.

Two limitations are associated with the current study. First, our method might be inappropriate for the in vivo imaging of βG-expressing tumors that reside near the gallbladder and intestines, since these organs display strong signals after injection of the radioiodinated probes. Although some preventive manipulations are suggested, their efficacy remains to be verified. Second, the small sample size has rendered data interpretation difficult. For example, although retention of radioactivity in CT26 versus CT26/βG tumors at 1 hour after injection is visually different, it was not statistically significant. Future

Figure 6

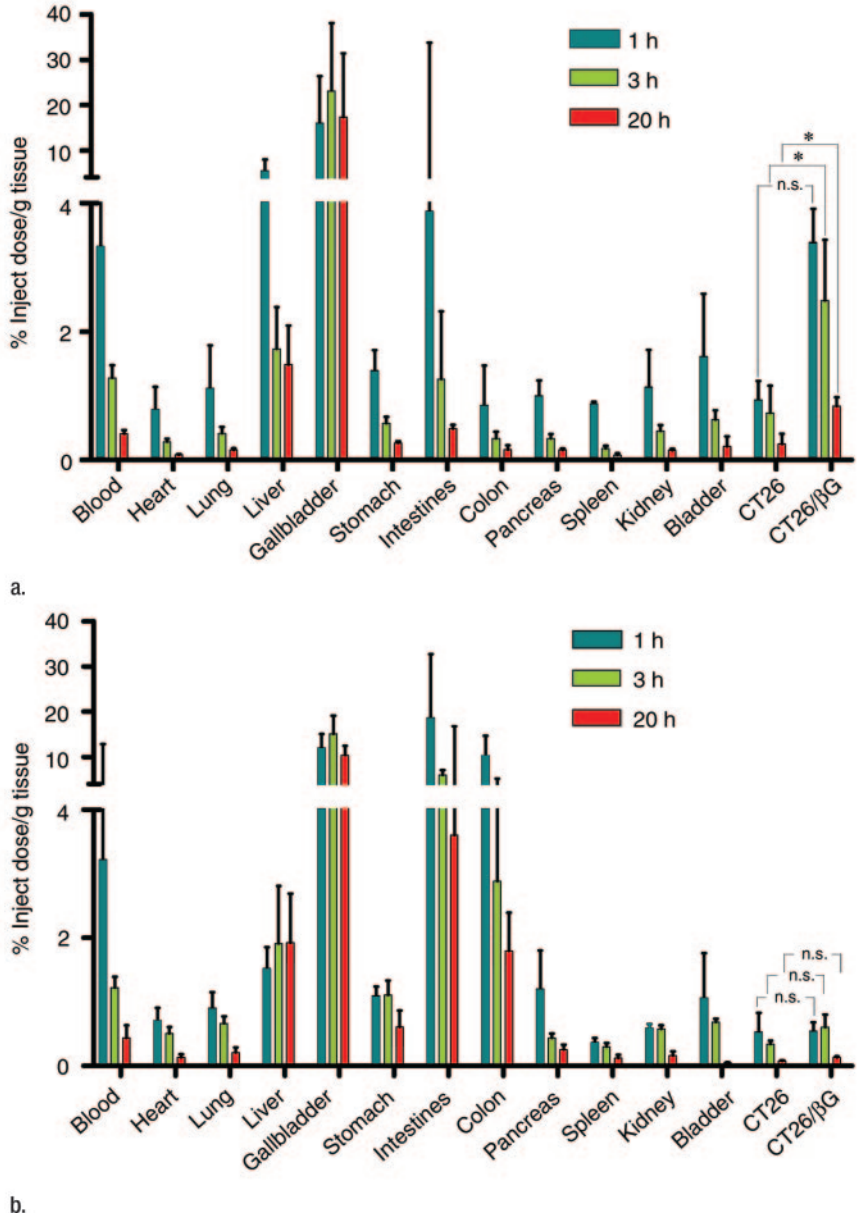

Figure 6: Graphs show biodistribution of **(a)** ^{131}I-PTH-G and **(b)** ^{131}I-PTH in selected organs in mice bearing CT26/βG or parental CT26 tumors. Selected organs and tumors were removed from the mice after 1 (n = 3), 3 (n = 5), and 20 (n = 6) hours. Error bars = standard error of the mean. * = $P < .05$, *n.s.* = nonsignificant.

studies with larger sample sizes may clarify this issue.

In summary, molecular imaging is a promising method to pair diagnosis and therapy for personalized medicine, which is especially useful in cancer therapy because of the many different molecular mechanisms that can cause this disease. We have developed a ^{124}I-PTH-G probe for micro-PET imaging of βG activity by the specific conversion and accumulation of hydrophobic ^{124}I-PTH in βG-expressing tumor sites. Importantly, our strategy is designed for the PET imaging system, which is currently the state-of-the-art technology in tumor detection. Thus, the development of new glucuronide PET probes should complement the detection capability that can diagnose βG-expressing cancers. Successful development of proactive glucuronide probes is expected to pair the diagnosis of βG activity and glucuronide prodrug targeted therapy for improved personalized health care.

Acknowledgment: The authors acknowledge technical support from the National Sun Yat-Sen University-Kaohsiung Medical University Joint Research Center.

References

1. Haisma HJ, van Muijen M, Pinedo HM, Boven E. Comparison of two anthracycline-based prodrugs for activation by a monoclonal antibody-beta-glucuronidase conjugate in the specific treatment of cancer. Cell Biophys 1994;24–25:185–192.
2. Houba PH, Boven E, van der Meulen-Muileman IH, et al. A novel doxorubicin-glucuronide prodrug DOX-GA3 for tumour-selective chemotherapy: distribution and efficacy in experimental human ovarian cancer. Br J Cancer 2001;84(4):550–557.
3. Schmidt F, Monneret C. Prodrug mono therapy: synthesis and biological evaluation of an etoposide glucuronide-prodrug. Bioorg Med Chem 2003;11(10):2277–2283.
4. Angenault S, Thirot S, Schmidt F, Monneret C, Pfeiffer B, Renard P. Cancer chemotherapy: a SN-38 (7-ethyl-10-hydroxycamptothecin) glucuronide prodrug for treatment by a PMT (Prodrug MonoTherapy) strategy. Bioorg Med Chem Lett 2003;13(5):947–950.
5. Leu YL, Roffler SR, Chern JW. Design and synthesis of water-soluble glucuronide derivatives of camptothecin for cancer prodrug monotherapy and antibody-directed enzyme prodrug therapy (ADEPT). J Med Chem 1999;42(18):3623–3628.
6. de Bont DB, Leenders RG, Haisma HJ, van der Meulen-Muileman I, Scheeren HW. Synthesis and biological activity of beta-glucuronyl carbamate-based prodrugs of paclitaxel as potential candidates for ADEPT. Bioorg Med Chem 1997;5(2):405–414.
7. Bouvier E, Thirot S, Schmidt F, Monneret C. First enzymatically activated Taxotere prodrugs designed for ADEPT and PMT. Bioorg Med Chem 2004;12(5):969–977.
8. Cheng TL, Chen BM, Chern JW, Wu MF, Roffler SR. Efficient clearance of poly(ethylene glycol)-modified immunoenzyme with anti-PEG monoclonal antibody for prodrug cancer therapy. Bioconjug Chem 2000; 11(2):258–266.
9. Wang SM, Chern JW, Yeh MY, Ng JC, Tung E, Roffler SR. Specific activation of glucuronide prodrugs by antibody-targeted enzyme conjugates for cancer therapy. Cancer Res 1992;52(16):4484–4491.
10. de Graaf M, Boven E, Scheeren HW, Haisma HJ, Pinedo HM. Beta-glucuronidase-mediated drug release. Curr Pharm Des 2002; 8(15):1391–1403.
11. Chen BM, Cheng TL, Tzou SC, Roffler SR. Potentiation of antitumor immunity by antibody-directed enzyme prodrug therapy. Int J Cancer 2001;94(6):850–858.
12. Chen KC, Cheng TL, Leu YL, et al. Membrane-localized activation of glucuronide prodrugs by beta-glucuronidase enzymes. Cancer Gene Ther 2007;14(2):187–200.
13. Chuang KH, Cheng CM, Roffler SR, et al. Combination cancer therapy by hapten-targeted prodrug-activating enzymes and cytokines. Bioconjug Chem 2006;17(3):707–714.
14. Hedley D, Ogilvie L, Springer C. Carboxypeptidase-G2-based gene-directed enzyme-prodrug therapy: a new weapon in the GDEPT armoury. Nat Rev Cancer 2007; 7(11):870–879.
15. Cheng CM, Lu YL, Chuang KH, et al. Tumor-targeting prodrug-activating bacteria for cancer therapy. Cancer Gene Ther 2008; 15(6):393–401.
16. Prijovich ZM, Chen BM, Leu YL, Chern JW, Roffler SR. Anti-tumour activity and toxicity of the new prodrug 9-aminocamptothecin glucuronide (9ACG) in mice. Br J Cancer 2002;86(10):1634–1638.
17. Bosslet K, Straub R, Blumrich M, et al. Elucidation of the mechanism enabling tumor selective prodrug monotherapy. Cancer Res 1998;58(6):1195–1201.
18. Connors TA, Whisson ME. Cure of mice bearing advanced plasma cell tumours with aniline mustard: the relationship between glucuronidase activity and tumour sensitivity. Nature 1966;210(5038):866–867.
19. Schumacher U, Adam E, Zangemeister-Wittke U, Gossrau R. Histochemistry of therapeutically relevant enzymes in human tumours transplanted into severe combined immunodeficient (SCID) mice: nitric oxide synthase-associated diaphorase, beta-D-glucuronidase and non-specific alkaline phosphatase. Acta Histochem 1996;98(4):381–387.
20. Kopen GC, Prockop DJ, Phinney DG. Enhanced in situ detection of beta-glucuronidase activity in murine tissue. J Histochem Cytochem 1999;47(7):965–968.
21. Lorincz M, Roederer M, Diwu Z, Herzenberg LA, Nolan GP. Enzyme-generated intracellular fluorescence for single-cell reporter gene analysis utilizing Escherichia coli beta-glucuronidase. Cytometry 1996;24(4):321–329.
22. Nimmo-Smith RH. p-Nitrophenyl-beta-glucuronide as substrate for beta-glucuronidase. Biochim Biophys Acta 1961;50:166–169.
23. Sperker B, Schick M, Kroemer HK. High-performance liquid chromatographic quantification of 4-methylumbelliferyl-beta-D-glucuronide as a probe for human beta-glucuronidase activity in tissue homogenates. J Chromatogr B Biomed Appl 1996;685(1): 181–184.
24. Su YC, Chuang KH, Wang YM, et al. Gene expression imaging by enzymatic catalysis of a fluorescent probe via membrane-anchored beta-glucuronidase. Gene Ther 2007;14(7): 565–574.
25. Sharkey RM, Karacay H, Vallabhajosula S, et al. Metastatic human colonic carcinoma: molecular imaging with pretargeted SPECT and PET in a mouse model. Radiology 2008; 246(2):497–507.
26. Diez T, Cabezas JA. Properties of two molecular forms of beta-glucuronidase from the mollusc Littorina littorea L. Eur J Biochem 1979;93(2):301–311.
27. Lin KJ, Ye XX, Yen TC, et al. Biodistribution study of [(123)I] ADAM in mice: correlation with whole body autoradiography. Nucl Med Biol 2002;29(6):643–650.
28. Hagenbuch B, Meier PJ. The superfamily of organic anion transporting polypeptides. Biochim Biophys Acta 2003;1609(1):1–18.
29. Smith NF, Figg WD, Sparreboom A. Role of the liver-specific transporters OATP1B1 and OATP1B3 in governing drug elimination. Expert Opin Drug Metab Toxicol 2005;1(3): 429–445.
30. Ishiguro N, Maeda K, Saito A, et al. Estab-

lishment of a set of double transfectants coexpressing organic anion transporting polypeptide 1B3 and hepatic efflux transporters for the characterization of the hepatobiliary transport of telmisartan acylglucuronide. Drug Metab Dispos 2008; 36(4):796–805.

31. Kanai N, Lu R, Bao Y, Wolkoff AW, Vore M, Schuster VL. Estradiol 17 beta-D-glucuronide is a high-affinity substrate for oatp organic anion transporter. Am J Physiol 1996; 270(2 pt 2):F326–F331.

32. Shitara Y, Li AP, Kato Y, et al. Function of uptake transporters for taurocholate and estradiol 17beta-D-glucuronide in cryopreserved human hepatocytes. Drug Metab Pharmacokinet 2003;18(1):33–41.

33. Gerk PM, Vore M. Regulation of expression of the multidrug resistance-associated protein 2 (MRP2) and its role in drug disposition. J Pharmacol Exp Ther 2002;302(2): 407–415.

34. Horikawa M, Kato Y, Tyson CA, Sugiyama Y. The potential for an interaction between MRP2 (ABCC2) and various therapeutic agents: probenecid as a candidate inhibitor of the biliary excretion of irinotecan metabolites. Drug Metab Pharmacokinet 2002; 17(1):23–33.

35. Jager W, Gehring E, Hagenauer B, Aust S, Senderowicz A, Thalhammer T. Biliary excretion of flavopiridol and its glucuronides in the isolated perfused rat liver: role of multidrug resistance protein 2 (Mrp2). Life Sci 2003;73(22):2841–2854.

36. Takasuna K, Hagiwara T, Watanabe K, et al. Optimal antidiarrhea treatment for antitumor agent irinotecan hydrochloride (CPT-11)-induced delayed diarrhea. Cancer Chemother Pharmacol 2006;58(4):494–503.

37. Ghanem CI, Ruiz ML, Villanueva SS, et al. Shift from biliary to urinary elimination of acetaminophen-glucuronide in acetaminophen-pretreated rats. J Pharmacol Exp Ther 2005;315(3):987–995.

38. Namkoong EM, Kim IW, Kim DD, Chung SJ, Shim CK. Effect of probenecid on the biliary excretion of belotecan. Arch Pharm Res 2007;30(11):1482–1488.

39. Ogasawara T, Takikawa H. Biliary excretion of phenolphthalein glucuronide in the rat. Hepatol Res 2001;20(2):221–231.

40. Schipper ML, Cheng Z, Lee SW, et al. micro-PET-based biodistribution of quantum dots in living mice. J Nucl Med 2007;48(9):1511–1518.

41. Al-Nahhas A, Win Z, Szyszko T, et al. Gallium-68 PET: a new frontier in receptor cancer imaging. Anticancer Res 2007; 27(6B):4087–4094.

42. Cheng TL, Chou WC, Chen BM, Chern JW, Roffler SR. Characterization of an antineoplastic glucuronide prodrug. Biochem Pharmacol 1999;58(2):325–328.

43. Haisma HJ, Boven E, van Muijen M, de Jong J, van der Vijgh WJ, Pinedo HM. A monoclonal antibody-beta-glucuronidase conjugate as activator of the prodrug epirubicin-glucuronide for specific treatment of cancer. Br J Cancer 1992;66(3):474–478.

44. Stahl PD, Fishman WH. Beta-glucuronidase. In: Bergmeyer J, Grassl M, eds. Methods in enzymatic analysis. Weinheim, Germany: Verlag Chemie, 1984; 246–256.

45. Duimstra JA, Femia FJ, Meade TJ. A gadolinium chelate for detection of beta-glucuronidase: a self-immolative approach. J Am Chem Soc 2005;127(37):12847–12855.